

Mimetic Black Holes

Mohammad Ali Gorji^{1,2} *, Alireza Allahyari² †, Mohsen Khodadi² ‡, Hassan Firouzjahi^{2,3} §

¹*Center for Gravitational Physics, Yukawa Institute for Theoretical Physics, Kyoto University,
Kyoto 606-8502, Japan*

²*School of Astronomy, Institute for Research in Fundamental Sciences (IPM),
P. O. Box 19395-5531, Tehran, Iran*

³*Department of Physics, Faculty of Basic Sciences, University of Mazandaran,
P. O. Box 47416-95447, Babolsar, Iran*

Abstract

In this paper, we look for the vacuum static spherically symmetric solution in the mimetic gravity scenario. The simplest solution possesses two naked singularities in which one of these singularities is due to caustics formation. However, we construct the mimetic black hole solution by gluing the exterior static spherically symmetric solution to a time-dependent anisotropic spacetime describing the interior of the black hole. It is shown that these two solutions match continuously on the surface of the event horizon. Some physical properties of the corresponding mimetic black hole solution are discussed.

*gorji@yukawa.kyoto-u.ac.jp

†alireza.al@ipm.ir

‡m.khodadi@ipm.ir

§frouz@ipm.ir

1 Introduction

Mimetic gravity is a scalar-tensor gravity in which the conformal mode of gravity is isolated by means of a scalar field [1]. Alternatively, the setup can be viewed as a special case of a general conformal/disformal transformation in which the transformation between the old and new metrics is degenerate. With a non-invertible conformal/disformal transformation the number of degrees of freedom can increase such that the longitudinal mode of gravity will become dynamical [2, 3, 4, 5]. The conformal transformation relating the physical metric $g_{\mu\nu}$ to the auxiliary metric $\tilde{g}_{\mu\nu}$ and the mimetic field ϕ is given by [1]¹

$$g_{\mu\nu} = \pm(\tilde{g}^{\alpha\beta}\partial_\alpha\phi\partial_\beta\phi)\tilde{g}_{\mu\nu}. \quad (1)$$

The above relation implies that the physical metric satisfies the following constraint

$$g^{\mu\nu}\partial_\mu\phi\partial_\nu\phi = \pm 1. \quad (2)$$

Therefore, the vector $\partial^\mu\phi$ is spacelike for the + sign while it is timelike for the – sign.

The most important point about the mimetic transformation (1) is that it is a singular transformation so that we cannot express the auxiliary metric $\tilde{g}_{\mu\nu}$ in terms of the physical metric $g_{\mu\nu}$ [2]. The resultant new degree of freedom associated with the transformation (1) represents the longitudinal mode of gravity which is dynamical even in the absence of any matter field. If we start with the vacuum Einstein-Hilbert action in terms of the physical metric $g_{\mu\nu}$ and then performing the mimetic transformation (1), we end up with a scalar-tensor theory in terms of the auxiliary metric $\tilde{g}_{\mu\nu}$ and dynamical scalar field ϕ [1]. Equivalently, one can work with the physical metric $g_{\mu\nu}$ and dynamical scalar field ϕ by taking the constraint Eq. (2) into account by means of a Lagrange multiplier as follows ² [6]

$$S_\pm = \int d^4x \sqrt{-g} \left[\frac{R}{2} + \lambda \left(g^{\mu\nu} \partial_\mu \phi \partial_\nu \phi \mp 1 \right) \right], \quad (3)$$

where R is the Ricci scalar constructed from the physical metric $g_{\mu\nu}$ while the auxiliary field λ enforces the mimetic constraint Eq. (2). We have allowed for the vector field $\partial^\mu\phi$ to be either spacelike or timelike which is described by the actions S_+ and S_- respectively.

The cosmological implications of the mimetic setup with the action S_- and the timelike vector $\partial^\mu\phi$ are widely studied in recent years [7, 8, 9, 10, 11, 12, 13, 14, 31]. Interestingly, an energy density component naturally arises in this scenario which behaves like dark matter so that λ and ϕ play the roles of energy density and velocity potential [1]. Due to the attractive nature of the resultant dark matter, the model finally ends up with caustic singularities [15, 16, 17]. This problem however would not arise in the context of mimetic gauge field scenario where the scalar field is replaced with a gauge field [18, 19, 20, 21]. Moreover, the sound speed for the scalar perturbations in mimetic dark matter scenario vanishes and in order to generate a propagating mode, it is suggested to add some higher derivative terms of the mimetic scalar field to the action [22, 23]. The resultant setup then suffers from the ghost and/or gradient instabilities [24, 25, 26] and one needs to add a non-minimal coupling between the higher derivatives of the mimetic scalar field and the curvature terms to make the setup stable [27, 28, 29, 30].

¹We work with the metric signature $(-, +, +, +)$.

²We work in units $M_P = 1/\sqrt{8\pi G} = 1$.

In this paper, we construct the black hole solution in the original mimetic scenario defined by the action Eq. (3). Some attempts have been made in this direction in the Refs. [32, 33, 34, 35, 36, 37]. But the difficult part is that in order to have a static black hole solution we need to have an event horizon. As we will show, obtaining an event horizon for a static black hole solution in the mimetic gravity scenario is not an easy task. More precisely, unlike in cosmological setups where one uses only the timelike vector $\partial^\mu\phi$, here we need both timelike and spacelike vectors $\partial^\mu\phi$. The reason is that a black hole would have an event horizon by definition and the vector $\partial^\mu\phi$ changes from a spacelike vector to a timelike vector after one crosses the horizon. As a result, we need both actions S_\pm in Eq. (3) in order to find a black hole solution in mimetic scenario.

2 Static Solution with Naked Singularities

In this section, our aim is to find a static spherically symmetric solution in the mimetic gravity scenario. We show that the static spherically symmetric solution is not a black hole solution but a spacetime with naked singularities. We present a black hole solution with a proper horizon in next Section.

The general scalar field and the the Einstein field equations are

$$\partial_\mu(\sqrt{-g}\lambda g^{\mu\nu}\partial_\nu\phi) = 0, \quad (4)$$

and

$$R_{\mu\nu} - \frac{1}{2}Rg_{\mu\nu} = -2\lambda\partial_\mu\phi\partial_\nu\phi, \quad (5)$$

where the mimetic constraint Eq. (2) has been imposed to simplify the last equation.

The metric in local coordinates (t, r, θ, φ) has the form

$$ds^2 = -A(r)dt^2 + \frac{dr^2}{B(r)} + r^2d\Omega^2, \quad (6)$$

where $A(r) > 0$ and $B(r) > 0$ are two unknown functions which should be determined after solving the corresponding dynamical equations and $d\Omega^2 = d\theta^2 + \sin^2\theta d\varphi^2$ is the metric of a sphere with unit radius.

For the scalar field and the auxiliary field we also consider the following static ansatz

$$\phi = \phi(r), \quad \lambda = \lambda(r). \quad (7)$$

Substituting from Eqs. (6) and (7) in mimetic constraint (2), we find

$$B\phi'^2 = \pm 1, \quad (8)$$

where a prime denotes the derivative with respect to r . Since $B > 0$, from Eq. (8) we conclude that we have to work with the action S_+ in which $\partial^\mu\phi$ is a spacelike vector. This shows that the static ansatz is consistent with S_+ but not with S_- . This is in agreement with the no-go result that is obtained in the context of Horava-Lifshitz gravity in [38]. Indeed, mimetic model

with timelike vector field $\partial^\mu\phi$ defined by S_- also emerges from the infrared (IR) limit of Horava-Lifshitz gravity and Einstein-aether scenario [39, 40]. Restricting ourselves to S_+ , from Eq. (8) we obtain

$$\phi' = \pm \frac{1}{\sqrt{B}}, \quad (9)$$

Without loss of generality we take the positive branch of solution in our forthcoming analysis.

The tt component of the Einstein equations (5) yields

$$\partial_r(rB) = 1, \quad (10)$$

where we have substituted from Eq. (9). Solving the above equation yields

$$B = 1 + \frac{c_0}{r}, \quad (11)$$

where c_0 is an integration constant.

Before continuing with the other components of the Einstein equations, it is helpful to look at the mimetic field equation (4) which in coordinates defined in Eq. (6) yields

$$\partial_r(\sqrt{A}r^2\lambda) = 0, \quad (12)$$

where we have used the fact that $\sqrt{-g} = \sqrt{A/B}r^2 \sin\theta$ and also substituted from Eq. (9). The above equation can be solved to give

$$A = \left(\frac{c_1}{r^2\lambda}\right)^2, \quad (13)$$

where c_1 is another integration constant. Note that A is always positive and, therefore, we would have $B > 0$. This confirms that the static solution can only be achieved in S_+ model.

Substituting Eqs. (9), (11) and (13) in the rr component of the Einstein equation, we find the following differential equation for the Lagrange multiplier λ ,

$$(r + c_0)\frac{\lambda'}{\lambda} + r^2\lambda + 2 + \frac{3c_0}{2r} = 0. \quad (14)$$

The above equation can be easily integrated yielding the following solution

$$\lambda = \frac{1}{2r^2} \left[1 - \sqrt{1 + c_0/r} \ln \left(\sqrt{r/c_2} (1 + \sqrt{1 + c_0/r}) \right) \right]^{-1}, \quad (15)$$

where c_2 is a constant of integration. From the above solution, we see that λ diverges at two points $r = 0$ and $r = r_f$ which solves the equation $1 = \sqrt{1 + c_0/r_f} \ln \left(\sqrt{r_f/c_2} (1 + \sqrt{1 + c_0/r_f}) \right)$. Solving this equation for c_2 and then substituting the result back in Eq. (15), we find

$$\lambda = \frac{1}{2r^2} \left[1 - \sqrt{1 + c_0/r} \left(\frac{1}{\sqrt{1 + c_0/r_f}} + \ln \sqrt{\frac{r}{r_f} \frac{1 + \sqrt{1 + c_0/r}}{1 + \sqrt{1 + c_0/r_f}}} \right) \right]^{-1}. \quad (16)$$

The behaviour of λ as a function of r is plotted in Fig. 1 which shows that there is a branch cut at $r = r_f$ so that λ changes sign with $\lim_{r \rightarrow r_f^-} \lambda = +\infty$ and $\lim_{r \rightarrow r_f^+} \lambda = -\infty$.

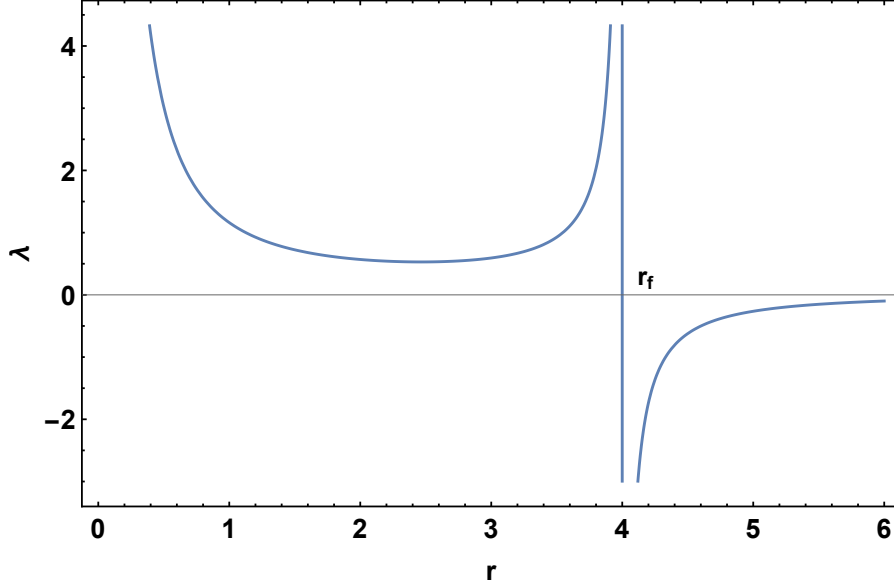


Figure 1: The plot of λ given in Eq. (16) versus the radial coordinate r for $c_0 = 2$ and $r_f = 4$. Since λ also characterizes the curvature invariants like Ricci scalar, we see that there is a singularity at $r = r_f$ after which the curvature changes sign. We show that $r = r_f$ is a caustic singularity while $r = 0$ is the usual curvature singularity.

To understand whether these divergences are genuine or the coordinate artifacts, we look at the curvature invariants. In the case of Schwarzschild black hole, the Ricci scalar and Ricci tensor both vanish so in order to investigate the singularity properties, one usually looks at the Kretschmann scalar $R_{\mu\nu\alpha\beta}R^{\mu\nu\alpha\beta}$. In our setup, however, the Ricci scalar and Ricci tensor are both non-zero so it is reasonable to first look at the scalar quantities constructed from them. Taking the trace of the Einstein equation (5) and using the mimetic constraint Eq. (2) for the spacelike case, we find

$$R = 2\lambda. \quad (17)$$

Substituting the above relation back into the Einstein equation (5), we find

$$R_{\mu\nu} = \lambda g_{\mu\nu} - 2\lambda \partial_\mu \phi \partial_\nu \phi. \quad (18)$$

In addition to the Ricci scalar which is given by (17), we can construct another scalar quantity from the Ricci tensor with the same dimension as follows

$$\partial^\mu \phi \partial^\nu \phi R_{\mu\nu} = \lambda. \quad (19)$$

The next nonzero scalar curvature which can be constructed is $R_{\mu\nu}R^{\mu\nu}$, which after using the mimetic constraint Eq. (2) in Eq. (18) yields

$$R_{\mu\nu}R^{\mu\nu} = 4\lambda^2. \quad (20)$$

We can also write the Kretschmann scalar in terms of λ as

$$R_{\mu\nu\alpha\beta}R^{\mu\nu\alpha\beta} = 12\lambda^2 - \frac{16\lambda c_0}{r^3} + \frac{12c_0^2}{r^6}, \quad (21)$$

while the Weyl squared scalar is given by

$$C_{\mu\nu\alpha\beta}C^{\mu\nu\alpha\beta} = \frac{16}{3} \left(\lambda - \frac{3c_0}{2r^3} \right)^2. \quad (22)$$

From the above relations we see that λ characterizes all curvature invariants and therefore the divergences at $r = 0$ and $r = r_f$ (see Fig. 1) are real singularities in this scenario. Since there is no event horizon in this solution, $r = 0$ and $r \rightarrow r_f$ are *naked singularities*. This is the the natural static spherically symmetric solution of the mimetic scenario.

If we only look at the curvature invariants, we cannot distinct between the two singularities $r = 0$ and $r = r_f$. It is then useful to look at $g_{tt} = -(4r^4\lambda^2)^{-1}$. From Eq. (16), it is clear that g_{tt} vanishes at r_f but not at $r = 0$. In Section 4 we will show that indeed the types of singularities at $r = 0$ and $r = r_f$ are totally different so that the first is the usual curvature singularity which also arises in the standard general relativity (much similar to what arises in the center of standard black hole solutions like Schwarzschild solution) while the latter is a caustic-type singularity which is the characteristic of the mimetic gravity scenario.

From Eq. (17) and Fig 1, we see that the two regions $r \in [0, r_f]$ and $r \in [r_f, \infty]$ describe regions with positive and negative curvatures respectively. We therefore take the positive region as our solution and choose r_f to be sufficiently large as $r_f \rightarrow \infty$ to exclude the region with negative curvature.

It is straightforward to show that all other Einstein's equations are satisfied and our solution is complete now. Substituting from Eqs. (11) and (13), the metric Eq. (6) takes the following form

$$ds^2 = -\frac{dt^2}{4r^4\lambda^2} + \frac{dr^2}{1 + \frac{c_0}{r}} + r^2 d\Omega^2, \quad (23)$$

where λ is given by Eq. (16). Now, substituting Eq. (16) in Eq. (13), we find an explicit solution for g_{tt} . We see that the effects of the constant c_1 can be absorbed through rescaling the time via $t \rightarrow t/c_1$ in metric (6) so on can set $c_1 = 1$ without loss of generality.

From Eqs. (8) and (13), we also see that g_{rr} and g_{tt} cannot change sign and, therefore, our solution (23) does not have any horizon. Consequently, our solution (23) does not describe a black hole. To get some intuition, it is useful to compare our solution with its standard counterpart, *i.e.*, the Schwarzschild solution. In Schwarzschild solution, $g_{tt} = -g^{rr} = -(1 + \frac{c_0}{r})$ so that g_{tt} is related to the Newtonian potential Φ in the weak field limit as $g_{tt} = -(1 + 2\Phi)$. We then conclude that c_0 should be negative which immediately implies the existence of a horizon since $g_{tt} = -g^{rr}$. In our solution (23) with $g_{tt} \neq -g^{rr}$, however, this is not the case. The reason is simple: contrary to GR the longitudinal mode of gravity encoded in the mimetic scalar field is dynamical here and has a non-zero profile in the whole spacetime. In other words, the energy of the mimetic scalar field is not localized and we cannot treat solution (23) as a gravitational field of an isolated source. Therefore, c_0 can be either positive or negative. We focus on the case of $c_0 > 0$ here and in the next section we will come back to the case of $c_0 < 0$ to construct a black hole solution.

In the case of $c_0 > 0$ from Eq. (11) we find that the condition $B > 0$ required by the mimetic constraint (8) is satisfied for $r \in [0, r_f]$. Therefore, the metric (23) is applicable for the whole range of $r \in [0, r_f]$ in this case.

Substituting Eq. (11) in Eq. (9) and then integrating, we find the following solution for the mimetic scalar field

$$\phi = r\sqrt{1 + c_0/r} - c_0 \ln \left(\sqrt{r/c_3} (1 + \sqrt{1 + c_0/r}) \right), \quad (24)$$

where c_3 is an integration constant. However, since our setup is shift-symmetric we can set $c_3 = 1$ without loss of generality.

Finally, it is useful to look at the special case of $c_0 = 0$ that corresponds to the Minkowski spacetime in the case of GR with the Schwarzschild solution. From (17) and (21), we see that the curvature invariants do not vanish even if we set $c_0 = 0$. Then, it is reasonable to consider the effects of c_0 coming from a local matter energy density while λ labels the effects coming from the energy density induced by mimetic field. In other words, we have a dynamical degrees of freedom even in the absence of any local matter energy density. Therefore, we do not have a Minkowski spacetime even far from a local matter profile. To see this fact explicitly, we set $c_0 = 0$ in our previous results in which the metric (23) takes the following simple form

$$ds^2 = - \left(\ln \frac{r}{r_f} \right)^2 dt^2 + dr^2 + r^2 d\Omega^2. \quad (25)$$

The above result shows that the metric is not asymptotically flat in the allowed region of $r \in [0, r_f)$. The above metric is not singular around $r = 0$ which shows that this singularity comes from the existence of a matter profile and disappears when we set $c_0 = 0$. The singularity at $r = r_f$ is, however, present even in the absence of any local matter field. This shows that the singularity at $r = r_f$ is the characteristic of the mimetic theory itself. We will show that the mimetic scenario approaches a caustic singularity at $r = r_f$ and we cannot trust the model near this point.

3 Black Hole Solution

In the previous Section we have shown that the static solution for the mimetic setup with the action S_+ and $\partial^\mu \phi$ being a spacelike four vector is not a black hole solution. It suffers from naked singularities if we suppose $c_0 > 0$ in Eq. (11) for $g_{rr} = B^{-1}$. The situation is different if we consider $c_0 < 0$ in which the requirement $B > 0$ from the mimetic constraint Eq. (8) implies that $r > |c_0|$. In the following subsections we study this case in details.

3.1 Exterior Static Spherically Symmetric Spacetime

To distinguish this solution with the metric (23), we work with the coordinates $(t_+, r_+, \theta, \varphi)$ in which the metric takes the form

$$ds_+^2 = -A_+(r_+)dt_+^2 + \frac{dr_+^2}{B_+(r_+)} + r_+^2 d\Omega^2. \quad (26)$$

We did not change the angular coordinates (θ, φ) since the changes are only for the temporal and radial coordinates. Moreover, we denote all functions with lower index $+$ in this subsection.

For $c_0 < 0$, the solution (11) can be written as

$$B_+ = 1 - \frac{2m_+}{r_+}, \quad (27)$$

where we have defined $c_0 = -2m_+$ with $m_+ > 0$ to be a positive constant. The spacetime then has an event horizon defined by $g^{r+r_+}(r_{+H}) = 0$ with

$$r_{+H} = 2m_+. \quad (28)$$

We note that the above solution is only applicable for $r_+ > 2m_+$ since $B_+ > 0$ for the spacelike vector $\partial^\mu \phi_+$.

All the solutions in the previous section are now applicable but restricted to the range $r_+ > 2m_+$. The metric takes the same form as Eq. (23) and

$$ds_+^2 = -\frac{dt_+^2}{4r_+^4 \lambda_+^2} + \frac{dr_+^2}{1 - \frac{2m_+}{r_+}} + r_+^2 d\Omega^2, \quad (29)$$

where λ_+ is given by (16) but replacing c_0 with $-2m_+$,

$$\lambda_+ = \frac{1}{2r_+^2} \left[1 - \sqrt{1 - \frac{2m_+}{r_+}} \left(\frac{1}{\sqrt{1 - \frac{2m_+}{r_f}}} + \ln \sqrt{\frac{r_+}{r_f}} \frac{1 + \sqrt{1 - \frac{2m_+}{r_+}}}{1 + \sqrt{1 - \frac{2m_+}{r_f}}} \right) \right]^{-1}. \quad (30)$$

The radial coordinate is restricted to the interval $r_+ \in [2m_+, r_f)$ where we also have fixed the constant c_1 in (13) such that $g_{t_+,t_+}(r_{+H}) = -4c_1^2 = -1$. This normalization does not affect the physical properties of the model since it only corresponds to rescaling the time via $t_+ \rightarrow t_+/c_1$.

The metric (29) can be thought as the exterior solution of a black hole with horizon r_{+H} defined in Eq. (28). To have a complete black hole solution, however, we need to find the interior solution as well. In the case of the Schwarzschild black hole in GR, the interior solution can be obtained by exchanging t and r coordinates in the exterior solution. More precisely, the interior solution can be obtained by solving Einstein's equation for a homogeneous but anisotropic background geometry. Here, we have to do the same. From the exterior metric (29), we see that by switching $t_+ \rightarrow r_-$ and $r_+ \rightarrow t_-$, we obtain a homogeneous but anisotropic metric for the interior solution. Considering a time-dependent anisotropic metric together with a time-dependent scalar $\phi(t)$ and auxiliary field $\lambda(t)$, it is easy to show that the spacelike action S_+ is not consistent with the mimetic constraint (2) and we have to use the timelike action S_- . In the next subsection, we show that the action S_- admits a time-dependent solution that matches the exterior solutions (29) and (30) on the null hypersurface of the event horizon.

3.2 Interior Solution

In this section, we focus on the timelike mimetic action S_- to find the interior solution in extension to the exterior solution obtained in the previous subsection. Working in local coordinates $(t_-, r_-, \theta, \varphi)$, we consider the following homogeneous but anisotropic background

$$ds_-^2 = -\frac{dt_-^2}{B_-(t_-)} + A_-(t_-) dr_-^2 + t_-^2 d\Omega^2, \quad (31)$$

where B_- and A_- are two unknown functions of t_- . We also consider the following time-dependent ansatz for the mimetic sector

$$\phi_- = \phi_-(t_-), \quad \lambda_- = \lambda_-(t_-), \quad (32)$$

which are consistent with the geometry (31). The mimetic constraint (2) for the timelike vector $\partial^\mu \phi$ then results in

$$\dot{\phi}_-^2 = \frac{1}{B_-}, \quad (33)$$

where a dot denotes the derivative with respect to t_- . Note that had we worked with the spacelike model S_+ , we would have found a minus sign in the right hand side of the above relation which was inconsistent with the assumption $B_- > 0$ in (31). This is the main reason why we should employ the timelike action S_- instead of the spacelike action S_+ when looking for the interior solution of the black hole.

Solving Eq. (33), we find

$$\dot{\phi}_- = \frac{1}{\sqrt{B_-}}, \quad (34)$$

where, without loss of generality, we took the positive branch in the above solution. The r_-r_- component of the Einstein equations (5) gives

$$\partial_{t_-}(t_- B_-) = -1, \quad (35)$$

where the substitution from Eq. (34) has been made. Solving the above equation gives

$$B_- = \frac{2m_-}{t_-} - 1, \quad (36)$$

where m_- is an integration constant. Here, m_- can be either positive or negative. We, however, are interested in an interior black hole solution so we take $m_- > 0$ which admits a horizon $B_-(t_{-H}) = 0$ at

$$t_{-H} = 2m_-. \quad (37)$$

The mimetic scalar field equation (4) gives

$$\partial_{t_-}(\sqrt{A_-} t_-^2 \lambda_-) = 0, \quad (38)$$

where again a substitution from Eq. (34) has been made. The above equation yields

$$A_- = \left(\frac{\tilde{c}_1}{t_-^2 \lambda_-} \right)^2, \quad (39)$$

where \tilde{c}_1 is an integration constant.

Substituting from Eqs. (34), (36) and (39) in the t_-t_- component of the Einstein equations (5) gives

$$(t_- - 2m_-) \frac{\dot{\lambda}_-}{\lambda_-} + t_-^2 \lambda_- + 2 - \frac{3m_-}{t_-} = 0. \quad (40)$$

The above first order differential equation can be integrated to give the following solution

$$\lambda_- = -\frac{1}{2t_-^2} \left[1 - \sqrt{\frac{2m_-}{t_-} - 1} \left(\arctan \sqrt{\frac{2m_-}{t_-} - 1} + \tilde{c}_2 \right) \right]^{-1}, \quad (41)$$

where \tilde{c}_2 is another constant of integration. The above solution shows that λ_- diverges at two times $t_- = 0$ and $t_- = t_i$ which is defined via $1 = \sqrt{\frac{2m_-}{t_i} - 1} \left(\arctan \sqrt{\frac{2m_-}{t_i} - 1} + \tilde{c}_2 \right)$. Solving this equation for \tilde{c}_2 and substituting the result back into the above solution, we find

$$\lambda_- = -\frac{1}{2t_-^2} \left[1 - \sqrt{\frac{2m_-}{t_-} - 1} \left(\frac{1}{\sqrt{\frac{2m_-}{t_i} - 1}} + \arctan \sqrt{\frac{2m_-}{t_-} - 1} - \arctan \sqrt{\frac{2m_-}{t_i} - 1} \right) \right]^{-1}. \quad (42)$$

Much similar to the discussion after Eq. (16), we can easily show that all curvature invariants diverge at the times $t_- = 0$ and $t_- = t_i$ and the region $t_- \in [0, t_i)$ corresponds to the negative curvature. We will discuss these singularities in details in Section 4.

Substituting Eq. (42) into Eq. (39), we see that the effects of constant \tilde{c}_1 can be removed in the metric (31) through re-scaling the radius via $r_- \rightarrow r_-/\tilde{c}_1$. However, note that $A_-(t_{-H}) = 4\tilde{c}_1^2$ so we set $\tilde{c}_1 = 1/2$ and $A_-(t_{-H}) = 1$. This is just a normalization and does not affect the physical properties of our solution.

Our solutions is complete for all dynamical fields and the metric (31) takes the following form

$$ds_-^2 = -\frac{dt_-^2}{\frac{2m_-}{t_-} - 1} + \frac{dr_-^2}{4t_-^4 \lambda_-^2} + t_-^2 d\Omega^2, \quad (43)$$

where the explicit form of λ_- is given by Eq. (42). Note that the above metric is only applicable for $t_- \in [t_i, 2m_-]$.

The homogeneous and *isotropic* solution of mimetic scenario in FLRW cosmological background is known as mimetic dark matter [1]. In order to compare the above homogeneous but *anisotropic* solution with its FLRW isotropic counterpart, in Appendix A we have presented our anisotropic solution in another chart which is more relevant for the cosmological purposes. The results resemble the isotropic cosmological solution in certain limits.

3.3 Junction Conditions: Gluing Exterior and Interior Solutions

We have found two different mimetic solutions in subsections 3.1 and 3.2. Our aim in this subsection is to check whether we can match the static spherically symmetric solution (29) with the homogeneous anisotropic time-dependent solution (43) as the exterior and interior of the mimetic black hole, respectively. In order to do this, we work with more general forms of metrics (26) and (31) which in particular cases reduce to our mimetic solutions (29) and (43). They are also applicable for the case of exterior and interior Schwarzschild solutions. The reason is that our solutions (29) and (43) are different from the Schwarzschild solution through A_\pm while the null hypersurfaces for metrics (26) and (31) are determined by B_\pm .

We have two different Lorentzian manifolds (\mathcal{M}_\pm, g_\pm) and in local coordinates $x^\mu = (t_\pm, r_\pm, \theta, \varphi)$, the corresponding line elements are given by metrics (26) and (31). The surfaces $\Sigma_\pm \subset \mathcal{M}$ defined by $r_+ = 2m_+$ for (26) and $t_- = 2m_-$ for (31) are determined by $B_\pm = 0$. The normal vectors $K_{\pm\mu}$ to null hypersurfaces Σ_\pm are given by

$$K_{+\mu} = \partial_\mu r_+ = \delta_\mu^{r_+}, \quad K_{-\mu} = \partial_\mu t_- = \delta_\mu^{t_-}. \quad (44)$$

From the above relations we can easily deduce that Σ_\pm are null hypersurfaces since

$$K_{\pm\mu} K_\pm^\mu = B_\pm = 0, \quad (45)$$

where B_\pm are evaluated at the horizons $r_+ = 2m_+$ and $t_- = 2m_-$ for Σ_\pm respectively.

Our aim is to glue the manifolds (\mathcal{M}_+, g_+) and (\mathcal{M}_-, g_-) on null hypersurfaces Σ_\pm where the junction conditions have to be imposed. The null hypersurfaces Σ_\pm are determined by the parametric equations $x_\pm^\mu(y^a)$ where we implement the coordinates $y^a = (s, \theta^A)$ which are applicable on both Σ_\pm . Here s is an arbitrary parameter which is not necessarily an affine parameter. The induced metrics h_\pm on Σ_\pm are the pullbacks of the embedding maps $\Sigma_\pm \rightarrow \mathcal{M}_\pm$ as

$$h_{\pm ab} = g_{\pm\mu\nu} e_{\pm a}^\mu e_{\pm b}^\nu, \quad (46)$$

where $e_{\pm a}^\mu \equiv \partial x_\pm^\mu / \partial y^a$ for null hypersurfaces with parametrization $dx_\pm^\mu = s K_\pm^\mu$ are,

$$e_{\pm s}^\mu = \left(\frac{\partial x_\pm^\mu}{\partial s} \right) \Big|_{\theta^A} = K_\pm^\mu, \quad e_{\pm A}^\mu = \left(\frac{\partial x_\pm^\mu}{\partial \theta^A} \right) \Big|_s, \quad (47)$$

which satisfy the condition (45) and also $K_{\pm\mu} e_{\pm A}^\mu = 0$. Using the above relations in Eq. (46), we find that $h_{ss} = 0 = h_{sA}$. We therefore deal with a two-dimensional induced metric

$$\sigma_{\pm AB} = g_{\pm\mu\nu} e_{\pm A}^\mu e_{\pm B}^\nu. \quad (48)$$

The first junction condition for the null hypersurfaces is

$$\sigma_{+AB}|_{\Sigma_+} = \sigma_{-AB}|_{\Sigma_-}. \quad (49)$$

Let us check that whether the above junction condition can be satisfied for our solutions (26) and (31). In our local coordinates, the tangent vectors are given by

$$e_{+s}^\mu = B_+ \delta_{r_+}^\mu, \quad e_{-s}^\mu = B_- \delta_{t_-}^\mu, \quad e_\theta^\mu = \delta_\theta^\mu, \quad e_\varphi^\mu = \delta_\varphi^\mu. \quad (50)$$

Substituting from the above relation and also Eqs. (26) and (31) into the first junction condition (49), it is straightforward to show that the junction condition is satisfied through the identification $r_+ \leftrightarrow t_-$ which was expected from the beginning.

In order to check the second junction condition, we need to find the transverse curvature

$$C_{\pm ab} \equiv \frac{1}{2} (N_{\pm\mu;\nu} + N_{\pm\nu;\mu}) e_{\pm a}^\mu e_{\pm b}^\nu, \quad (51)$$

where the null vectors N_\pm^μ are defined as

$$N_{\pm\mu} N_\pm^\mu = 0, \quad N_{\pm\mu} K_\pm^\mu = -1. \quad (52)$$

Substituting from Eqs. (26), (31), and (44) in above relations, we find the following solutions

$$N_+^\mu = \left(\mp \frac{1}{\sqrt{A_+ B_+}}, -1, 0, 0 \right), \quad N_-^\mu = \left(-1, \mp \frac{1}{\sqrt{A_- B_-}}, 0, 0 \right). \quad (53)$$

Correspondingly, substituting from Eqs. (47) in (51), we find the following nonzero components for the transverse curvature

$$\begin{aligned} C_{+11} &= \frac{B'_+}{2}, & C_{+22} &= -r_+, & C_{+33} &= -r_+ \sin^2 \theta, \\ C_{-11} &= -\frac{\dot{B}_-}{2}, & C_{-22} &= -t_-, & C_{-33} &= -t_- \sin^2 \theta. \end{aligned} \quad (54)$$

The second junction condition is given by

$$C_{+ab} = C_{-ab}. \quad (55)$$

It is straightforward to show that applying $r_+ \leftrightarrow t_-$, the above junction condition satisfies by the exterior and interior metrics (26) and (31) at horizons $r_+ = 2m_+$ and $t_- = 2m_-$ if we assume

$$m_+ = m_-. \quad (56)$$

In summary, we have shown that the exterior solution (26) and the interior solution (31) are matched smoothly on the null hypersurfaces $r_+ = 2m_+$ and $t_- = 2m_-$ where the junction conditions (49) and (55) are satisfied. We, therefore, have a black hole solution (\mathcal{M}, g, Σ) where $\mathcal{M} = \mathcal{M}_+ \cup \mathcal{M}_-$, $g = g_+ \cup g_-$, and $\Sigma = \Sigma_\pm$ is the associated horizon.

4 Caustic Singularities in the Mimetic Black Hole

In the previous section, we have constructed the mimetic black hole solution by gluing two different solutions. In this section, we investigate the physical properties of this mimetic black hole.

Let us first summarize the results from the previous section. The exterior metric has the following static spherically symmetric form

$$ds^2 = -\frac{dt^2}{4r^4 \lambda_+^2} + \frac{dr^2}{1 - \frac{2m}{r}} + r^2 d\Omega^2, \quad (57)$$

where λ_+ is given by Eq. (30) replacing now r_+ with r and m_+ with m . The interior solution is also given by

$$ds^2 = -\frac{dt^2}{\frac{2m}{t} - 1} + \frac{dr^2}{4t^4 \lambda_-^2} + t^2 d\Omega^2, \quad (58)$$

where λ_- is given by Eq. (41) replacing t_- with t and m_- with m .

After satisfying the junction conditions, we expect that all curvature invariants to be continuous across the surface of horizon. However, it is instructive to check this explicitly. This is easy to verify in our setup since all curvature invariants (17), (20), (21) and (22) are characterized

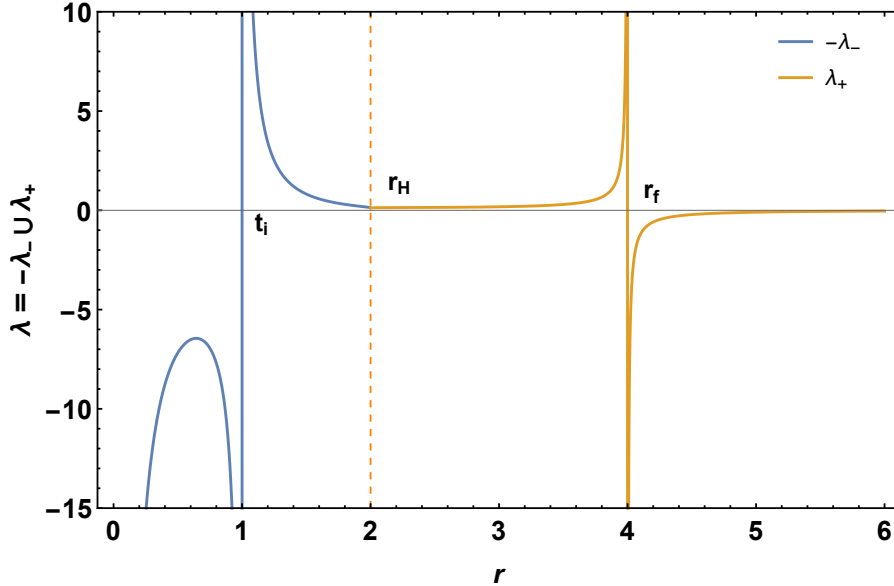


Figure 2: The plot of $\lambda = -\lambda_- \cup \lambda_+$ for $m = 1$, $t_i = 1$ and $r_f = 4$. We see that λ is continuous across the surface of horizon at $r = 2$. We deal with the black hole region $[t_i, 2m] \cup [2m, r_f]$.

by the auxiliary field λ so we only need to check the continuity of λ on the surface of horizon. For the exterior solution (29) all curvature invariants are the same as those obtained in Eqs. (17)-(22) via replacing $\lambda = \lambda_+$ where λ_+ is given by (30). In the case of the interior solution (43), it is straightforward to check that all curvature invariants are obtained by replacing $\lambda \rightarrow -\lambda_-$ where λ_- is given by Eq. (42). Note that we have identified $m_+ = m_- = m$. It is easy then to verify that

$$\lambda_+|_{\Sigma} = -\lambda_-|_{\Sigma}, \quad (59)$$

which shows the continuity of the auxiliary field and hence all curvature invariants are continuous across the surface of the horizon. The above relation holds irrespective of the values of t_i and r_f . In Fig. 2 we have plotted the combined auxiliary field $\lambda = -\lambda_- \cup \lambda_+$ which confirms that $-\lambda_-$ matches to λ_+ at the surface of the event horizon.

Now, we study the type of singularities at $t = t_i$ and $r = r_f$ that occur in our mimetic black hole solution (see Fig 2). Let us first study the singularity at $t = t_i$ for the interior solution (58). We first note that the timelike vector $n^\mu = \partial^\mu \phi$ is orthogonal to the constant-time hypersurfaces and it is also normalized through the mimetic constraint Eq. (2) as $n_\mu n^\mu = -1$. This vector then satisfies the geodesics equation

$$n^\mu \nabla_\mu n_\nu = 0. \quad (60)$$

Since a congruence of geodesics generally forms caustics, the above result shows that timelike hypersurfaces in mimetic setup with the action S_- develop caustics. Our second aim is to show when and where these caustic singularities occur. In other words, from the above general result we cannot conclude that which of $t = 0$ or $t = t_i$ is the time when caustics form. We therefore look at the metric (58) noting that at the time $t = t_i$, g_{rr} vanishes while it does not vanish at $t = 0$. Therefore, caustics with spherical symmetry are formed at finite time $t = t_i$ everywhere in background (see section 3 of Ref. [15] for the similar caustic singularities that form in Minkowski

spacetime with planar symmetry). Moreover, the second derivative (and higher derivative) of the field are characterized by the curvature invariants and the behaviour of all curvature invariants are given by λ . From Fig 2, we see that λ and therefore all curvature invariants diverge(s) at the caustic points. Note that curvature invariants (or equivalently λ) also diverge at the point of standard singularity $t = 0$ but g_{rr} does not vanish there which shows that $t = 0$ is not a caustic singularity. This is consistent with the intuitive discussions at the end of Section 2.

A similar arguments can be applied to the exterior solution (57). The vector $\partial^\mu \phi$ is orthogonal to constant- r (timelike) hypersurfaces and it is normalized through the mimetic constraint Eq. (2) as $n_\mu n^\mu = 1$. Again we conclude that n^μ satisfies the geodesic equation (60) and we would have caustic singularities. To see when and where they occur, we look at the exterior metric (57) where g_{tt} vanish at $r = r_f$. We therefore conclude that, in contrast with the interior case, there are caustic singularities within *finite radius* of r_f for all time in the background. The caustic singularities are localized at a finite radius for the exterior solution while they occur everywhere for the interior solution.

The general proof based on the geodesic equation (60) shows that caustic singularities are inevitable in both mimetic solutions defined by the actions S_\pm in (3). Although we have studied the details of caustic singularities in the case of spherical symmetric and anisotropic time-dependent backgrounds, the above proof shows that the existence of these singularities is independent of the background. The Appearance of caustics is not pathological for an effective field theory while it is a serious problem for a fundamental theory. Much similar to the metric field, the scalar field ϕ is a fundamental field in mimetic scenario which can couple to Standard Model fields. The mimetic scenario then breaks down near the caustics singularities. This problem can be solved if we suppose that the mimetic theory is an effective field theory which only emerges at low energies in the IR regime. Then, the appearance of the caustics signals for the emergence of a new physics at ultraviolet (UV) regime. In this regards, there would be a UV completion theory for the mimetic scenario which governs high curvature regime and prevents the formation of caustics. In the case of S_- , indeed, Horava-Lifshitz gravity can be thought as a UV completion theory [24]. Interestingly, caustics would not form at high curvature regimes in the Horava-Lifshitz gravity scenario (see Ref. [15] for the details). A similar UV completion theory, but with different foliations (in comparison with the spacelike foliation in Horava-Lifshitz gravity) which respects the symmetries of S_+ can potentially prevent the formation of caustics in the exterior solution. In this paper, however, we treat mimetic gravity as an effective theory and restrict ourselves to the low curvature regime of $[t'_i, 2m] \cup [2m, r'_f]$ with $t'_i \gg t_i$ and $r'_f \ll r_f$ so t'_i and r'_f are sufficiently far from the points of caustic singularities t_i and r_f . Moreover, as we have already mentioned, the intervals $0 < t < t_i$ and $r_f < r < \infty$ have negative curvatures and therefore they are physically different than the region $[t_i, 2m] \cup [2m, r_f]$ which posses positive curvature.

To get some physical intuition, it is useful to model the effects of mimetic field by a fluid. Let us start with the interior solution which looks like an anisotropic cosmological model. The right hand side of the Einstein equations (5) can be viewed as an effective energy-momentum tensor which has the same covariant form for both S_+ and S_- actions. Substituting from Eqs. (34) and (43), we find that for the interior solution $T^\mu_\nu = \text{diag}(2\lambda, 0, 0, 0)$. This shows that the energy density is given by $\rho = -2\lambda$ while the pressure vanishes. Vanishing pressure in region $t_i < t < 2m$ is the signature of attractive gravity which usually leads to caustic singularity within finite time as we have already mentioned. Since $\lambda > 0$ for $0 < t < t_i$, this region corresponds to

negative energy density $\rho < 0$ which is not allowed physically. Similarly, the region $r_f < r < \infty$ is the exterior counterpart of the interior region $0 < t < t_i$. However, we cannot model it by a known matter field. More precisely, substituting from Eqs. (9) and (29), we find that for the exterior region $T_\nu^\mu = \text{diag}(0, -2\lambda, 0, 0)$, which for the region $r_f < r < \infty$, represents a fluid with a negative pressure and vanishing energy density. Although this is not pathological but we do not know any realistic matter field (fluid) which represents this kind of property.

One important issue for any black hole solution is its thermodynamic properties which are associated to the black hole's Killing horizon. We therefore look at the Killing vectors of the exterior and interior solutions. For the exterior solution (57), there are four Killing vectors among which three of them are associated with the spherical symmetry and one corresponds to the static nature of the metric with the Killing vector $\mathcal{R}^\mu = \delta_t^\mu$ which we are interested in. Similarly, for the interior solution (58), $\mathcal{T}^\mu = \delta_r^\mu$ is a Killing vector that corresponds to the fact that the solution is r -independent. From Eqs. (57) and (58), we then find that

$$\mathcal{R}_\mu \mathcal{R}^\mu = g_{tt} = -\frac{1}{4r^2 \lambda_+^2}, \quad (61)$$

$$\mathcal{T}_\mu \mathcal{T}^\mu = g_{rr} = \frac{1}{4t^2 \lambda_-^2}. \quad (62)$$

The Killing horizon is defined as the location of the points where the magnitude of the Killing vectors vanish. From Eqs. (30) and (42) we see that the above Killing vectors vanish only asymptotically as

$$\mathcal{R}_\mu \mathcal{R}^\mu|_{r=r_f} = -\frac{1}{4r_f^2 \lambda_+^2(r_f)} \rightarrow 0 \quad (63)$$

$$\mathcal{T}_\mu \mathcal{T}^\mu|_{t=t_i} = \frac{1}{4t_i^2 \lambda_-^2(t_i)} \rightarrow 0. \quad (64)$$

We see that at the surfaces of caustic singularities, $r = r_f$ and $t = t_i$, Killing vectors become null since $|\lambda_\pm| \rightarrow \infty$. Therefore, the surfaces of caustic singularities are Killing horizons with infinite redshifts. This should be compared with the case of Schwarzschild solution in GR where the surface of infinite redshift coincides with the surface of event horizon while in the case of mimetic black hole there exist two surfaces of infinite redshift which are different than the surface of event horizon. Since the notion of surface gravity is related to the Killing horizon and not to event horizon, we therefore cannot associate any Hawking radiation to the event horizon of this mimetic black hole. Moreover, although it seems that we can associate thermodynamic properties to the surfaces $r = r_f$ and $t = t_i$ with caustic singularities, but one should be careful that our solution are not trusted near these points. As we already mentioned, the mimetic scenario breaks down near these points and one needs a UV completion to understand physics around and beyond these points.

5 Summary and Conclusions

Mimetic scenario is a conformal extension of general relativity in which the longitudinal mode of gravity, encoded in the mimetic scalar field ϕ , becomes dynamical even in the absence of

any matter field. This extra degree of freedom plays the roles of dark matter in a cosmological background.

In this paper, we have focused on the static spherically symmetric background to see whether the mimetic setup can admit a black hole solution. Contrary to the Schwarzschild solution in GR, this static solution is not a black hole but a spacetime with naked singularities. We have shown that one of these singularities is caustic type. The mimetic theory then breaks down near the caustic singularity. We have concluded that there is no natural black hole solution in the mimetic gravity scenario since we have to choose $\partial^\mu\phi$ to be a spacelike or a timelike vector field from the beginning while we need this vector field to change from a spacelike signature to a timelike signature or vice versa across the event horizon.

To resolve this problem, we then considered two types of mimetic models with the actions S_+ and S_- in which the vector $\partial^\mu\phi$ is spacelike in S_+ while it is timelike in S_- . We have shown that the first setup admits a static spherically symmetric solution with a horizon while the latter admits a time-dependent homogeneous anisotropic solution with a horizon. We have verified that these two different solutions (metrics (57) and (58) for the exterior and interior respectively) can be glued at their joint horizon leading to a mimetic black hole solution. Both of the exterior and interior solutions suffer from caustic singularities at high curvature regime. The mimetic scenario then would be considered as an effective theory which is applicable in the IR regime and breaks down near the caustic singularities. One then needs a UV-completion theory for the mimetic scenario near the caustic singularities. In the case of interior solution, the Horava-Lifshitz theory can be considered as a UV-completion of the timelike mimetic model S_- . Inspired by this fact, for the spacelike mimetic model S_+ , we speculated that a UV-completion theory similar to the the Horava-Lifshitz but with different foliation can be constructed. However, we do not know such a scenario.

There are two different Killing horizons for this black hole solution in which non of them coincides with the event horizon. Therefore, there is no notion of Hawking radiation to be associated to the event horizon. One needs to look for Hawking radiation at Killing horizons which turned out to be singular hypersurfaces due to caustics formation. The formation of caustics usually signals for a new physics and one can not trust mimetic scenario near these singular hypersurfaces.

Acknowledgments: We would like to thank Shinji Mukohyama for correspondence and comments on the draft and S. Ali Hosseini Mansoori for useful discussions. The work of M. A. G. was supported by Japan Society for the Promotion of Science (JSPS) Grants-in-Aid for international research fellow No. 19F19313.

A Anisotropic Mimetic Cosmologies

In order to obtain an interior solution for our black hole, we have considered mimetic model S_- with homogeneous *anisotropic* metric ansatz (31) in local coordinates $(t_-, r_-, \theta, \varphi)$

$$ds^2 = -\frac{dt^2}{B_-(t)} + A_-(t)dr^2 + t^2 d\Omega^2, \quad (65)$$

where we have identified (t_-, r_-) with (t, r) for the sake of simplicity which is consistent with the notation that we have used in Section 4. The local coordinates used in (65) was more apt in gluing the exterior (29) and interior (43) solutions. On the other hand, we know that the homogeneous *isotropic* cosmological solution for the mimetic model S_- is the mimetic dark matter in a FLRW background [1]. In order to compare our anisotropic results with its isotropic counterpart, it is better to work in another coordinates. In this respect, we consider the following Kantowski-Sachs spacetime

$$ds^2 = -dT^2 + X(T)^2 dr^2 + Y(T)^2 d\Omega^2, \quad (66)$$

where the new time coordinate is defined as

$$dT = \frac{dt}{\sqrt{B_-}}, \quad (67)$$

and $X(T) \equiv \sqrt{A_-(T)}$ and $Y(T) \equiv t(T)$ are two scale factors. To see the relation between the new time coordinate T and the old time coordinate t , we substitute from (36) and then integrate (67) to obtain

$$T = -\sqrt{t}\sqrt{2m-t} - m \arctan\left(-\frac{t-m}{\sqrt{t}\sqrt{2m-t}}\right), \quad (68)$$

where we have set a constant of integration to zero which corresponds to a shift in T . From the above solution, we see that $T \in [-\frac{m\pi}{2}, +\frac{m\pi}{2}]$ for $t \in [0, 2m]$. In Fig. (3), we have plotted T as a function of t/m . From Eq. (42), we know that $t = t_i$ is an arbitrary constant which determines the time that separates two regions with different curvatures. We have discussed that the region $t \in [0, t_i)$ violates the energy conditions if we model the mimetic field with a fluid with vanishing pressure. Therefore, on the physical ground, it is reasonable to identify $t = t_i$ with $T = 0$ and restrict ourselves to the positive branch of T so that $T \in [0, +\frac{m\pi}{2}]$.

From Eqs. (32) and (67), we see that the consistent ansatz for the metric (66) would be

$$\phi = \phi(T), \quad \lambda_- = \lambda_-(T). \quad (69)$$

Substituting Eq. (69) together with Eq. (66) in the mimetic constraint Eq. (2) for the S_- model, we find $(d\phi/dT)^2 = 1$ that after integration yields

$$\phi(T) = T, \quad (70)$$

where we have chosen the plus sign in the above solution.

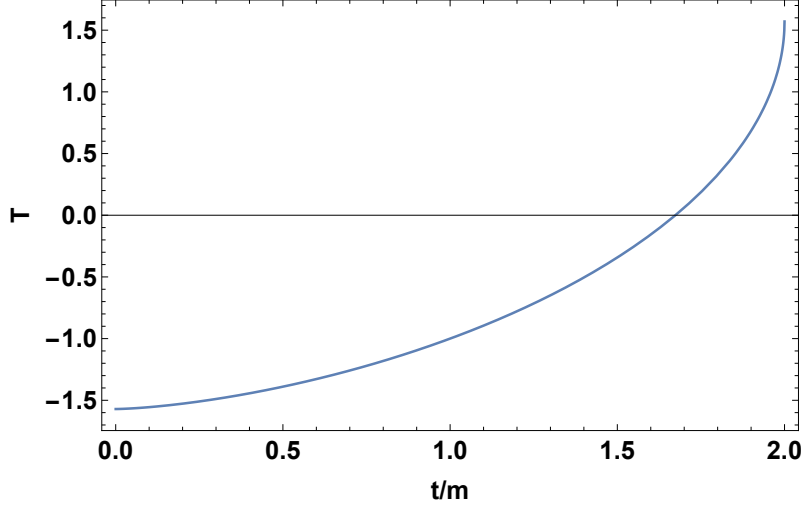


Figure 3: The new time coordinates T as a function of the old time coordinate t/m . We identify $T = 0$ with $t = t_i$ so that our solutions here with $T \in [0, +\frac{m\pi}{2}]$ covers $t \in [t_i, 2m]$ in Fig. 2, corresponding to the interior of the black hole.

The equation of motion for the mimetic scalar field from Eq. (4) then yields

$$X(T) = \frac{C_1}{Y(T)^2 \lambda_-(T)}, \quad (71)$$

where C_1 is a constant of integration.

The TT and rr components of the Einstein equations give

$$2(XY)^{-1} \frac{dX}{dT} \frac{dY}{dT} + Y^{-2} \left(1 + \left(\frac{dY}{dT} \right)^2 \right) = -2\lambda_-, \quad (72)$$

and

$$2Y \frac{d^2 Y}{dT^2} + \left(\frac{dY}{dT} \right)^2 + 1 = 0. \quad (73)$$

The solution to Eq. (73) is given in terms of the inverse function $f^{-1}(T)$ as follows

$$Y(T) = f^{-1}(T); \quad f(T) = 2C_2 \arctan \left(\frac{\sqrt{T}}{\sqrt{2C_2 - T}} \right) - \sqrt{2C_2 T - T^2}, \quad (74)$$

where C_2 is another integration constant. Identifying the point $T = 2C_2$ with $t = 2m$, from (68) we find that $C_2 = m\pi/4$.

Substituting Eq. (74) into Eqs. (71) and (72), we can solve for both X and λ_- as a function of T . Having obtained these solutions, our dynamical system is completely solved. We have plotted the solutions for X^2 , Y^2 , and λ_- as functions of T in Fig. 4. From Fig 2 we see that at $T = 0$, $X, Y \rightarrow 0$ and $\lambda \rightarrow \infty$. These results can be directly confirmed from the equations (71)-(74). From (74), we see that $Y(T = 0) = f^{-1}(T = 0) = 0$. Substituting (71) and (74) in (15) and then solving for $X(T)$, it is straightforward to show that $X \propto T^{2/3}$ in the limit $T \rightarrow 0$ and

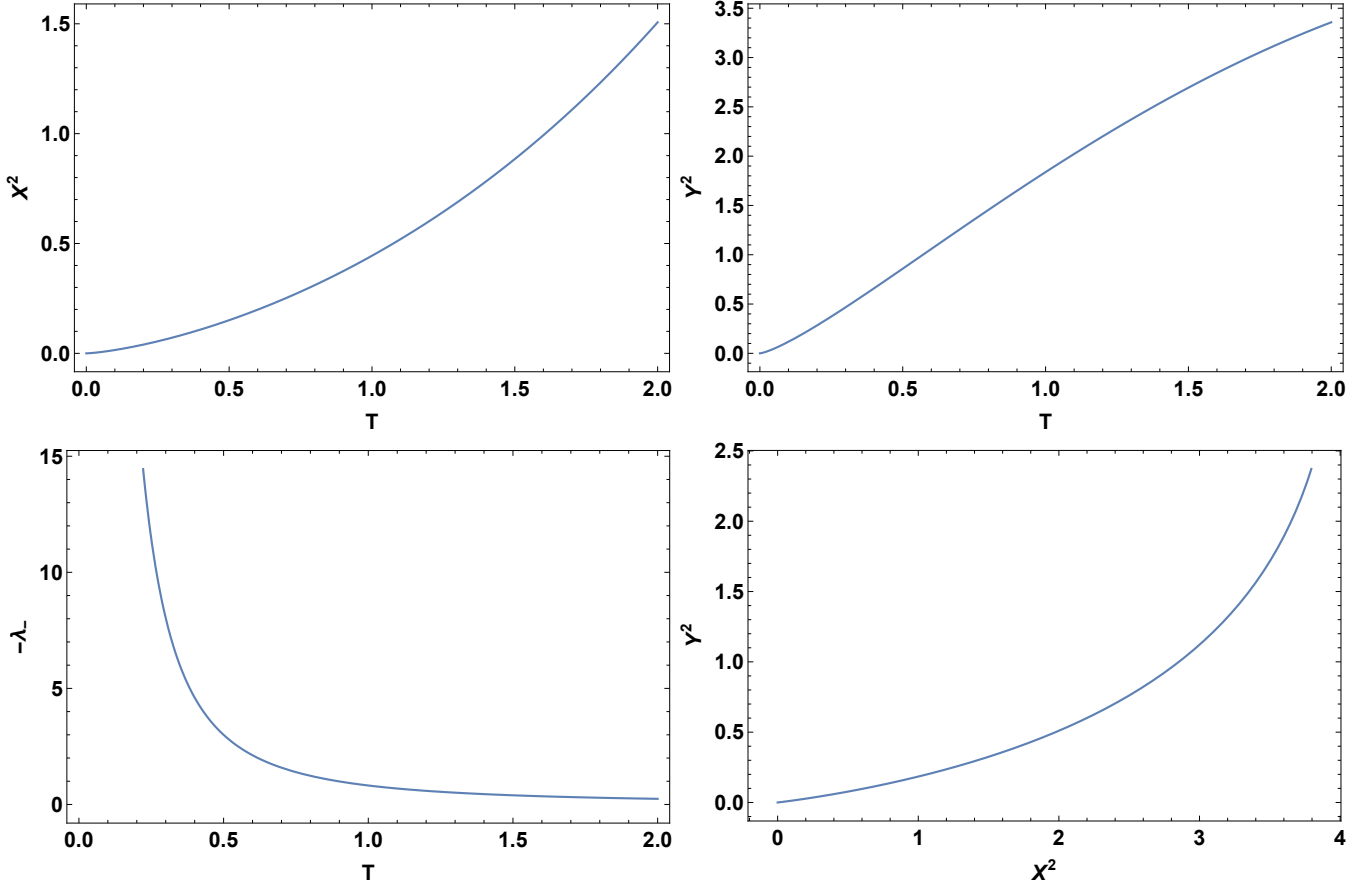


Figure 4: The plots of X^2 (top left), Y^2 (top right), $-\lambda_-$ (bottom left) as functions of T and the plot of X^2 vs. Y^2 (bottom right). As the scale factors shrink to zero, the energy density of the mimetic field diverges producing caustic singularities. X^2 and Y^2 both expand or contract simultaneously. The behavior of $-\lambda_-$ shows that the solution in this coordinate covers only $t_i < t$. The figures are plotted for $C_1 = 1 = C_2$.

therefore $X(T = 0) = 0$. This singularity is nothing but the formation of caustics. The metric components g_{rr} , $g_{\theta\theta}$, and $g_{\varphi,\varphi}$ all vanish in metric (66) at $T = 0$ while all curvature invariants, which are proportional to the second derivative of metric, diverge since they are characterized by λ . Therefore caustics form at the finite time $T = 0$ everywhere in the background.

Let us now compare the results of this appendix with those obtained for mimetic dark matter scenario in FLRW background [1]. First of all, the metric (66) becomes isotropic for $X \propto Y$ and then X (or Y) plays the roles of the scale factor $a(T)$ in FLRW background. In this limit, from Eq. (71) we find $\lambda_- \propto X^{-3} \propto a^{-3}$ which shows that the energy density $\rho = -2\lambda_- \propto a^{-3}$. This is nothing but the dark matter energy density. This can also be seen if we look at the metric (66) in the limit of small T

$$ds^2 \approx -dT^2 + \frac{T^{\frac{4}{3}}}{6^{\frac{2}{3}}C_2^{\frac{4}{3}}} \left(dr^2 + 9C_2^2 d\Omega^2 \right). \quad (75)$$

The above metric shows that for small T , the spacetime in the vicinity of the singularity $T = 0$

(which corresponds to $t = t_i$ in Fig. 2) behaves like a matter dominated universe with the scale factor $a(T) \sim T^{\frac{2}{3}}$, as expected.

Moreover, we note that due to the presence of a dark matter-like fluid, the metric (75) is contracting in both r and (θ, φ) directions. This is in contrast to the Schwarzschild solution for the interior of the black hole which is expanding along the r direction but contracting in (θ, φ) directions. It also signals the formation of caustic singularities due to the attractive nature of dark matter-like fluid.

References

- [1] A. H. Chamseddine and V. Mukhanov, JHEP **1311**, 135 (2013), [arXiv:1308.5410 [astro-ph.CO]].
- [2] N. Deruelle and J. Rua, JCAP **1409**, 002 (2014), [arXiv:1407.0825 [gr-qc]].
- [3] G. Domnech, S. Mukohyama, R. Namba, A. Naruko, R. Saitou and Y. Watanabe, Phys. Rev. D **92**, no. 8, 084027 (2015), [arXiv:1507.05390 [hep-th]].
- [4] H. Firouzjahi, M. A. Gorji, S. A. Hosseini Mansoori, A. Karami and T. Rostami, JCAP **1811**, 046 (2018) doi:10.1088/1475-7516/2018/11/046 [arXiv:1806.11472 [gr-qc]].
- [5] L. Shen, Y. Zheng and M. Li, arXiv:1909.01248 [gr-qc].
- [6] A. Golovnev, Phys. Lett. B **728**, 39 (2014), [arXiv:1310.2790 [gr-qc]].
- [7] F. Arroja, N. Bartolo, P. Karmakar and S. Matarrese, JCAP **1509**, 051 (2015), [arXiv:1506.08575 [gr-qc]].
- [8] N. Sadeghnezhad and K. Nozari, Phys. Lett. B **769**, 134 (2017), [arXiv:1703.06269 [gr-qc]].
- [9] D. Langlois, H. Liu, K. Noui and E. Wilson-Ewing, Class. Quant. Grav. **34**, no. 22, 225004 (2017), [arXiv:1703.10812 [gr-qc]].
- [10] J. Dutta, W. Khylllep, E. N. Saridakis, N. Tamanini and S. Vagnozzi, JCAP **1802**, 041 (2018), [arXiv:1711.07290 [gr-qc]].
- [11] A. Casalino, M. Rinaldi, L. Sebastiani and S. Vagnozzi, Phys. Dark Univ. **22**, 108 (2018), [arXiv:1803.02620 [gr-qc]].
- [12] S. Brahma, A. Golovnev and D. H. Yeom, Phys. Lett. B **782**, 280 (2018), [arXiv:1803.03955 [gr-qc]].
- [13] J. de Haro, L. Arest Sal and S. Pan, Gen. Rel. Grav. **51**, no. 4, 49 (2019), [arXiv:1803.09653 [gr-qc]].
- [14] M. de Cesare, Phys. Rev. D **99**, no. 6, 063505 (2019), [arXiv:1812.06171 [gr-qc]].
- [15] S. Mukohyama, JCAP **0909**, 005 (2009) doi:10.1088/1475-7516/2009/09/005 [arXiv:0906.5069 [hep-th]].

- [16] A. O. Barvinsky, JCAP **1401**, 014 (2014) doi:10.1088/1475-7516/2014/01/014 [arXiv:1311.3111 [hep-th]].
- [17] F. Capela and S. Ramazanov, JCAP **1504**, 051 (2015), [arXiv:1412.2051 [astro-ph.CO]].
- [18] A. Vikman, arXiv:1712.10311 [astro-ph.CO].
- [19] M. A. Gorji, S. Mukohyama, H. Firouzjahi and S. A. Hosseini Mansoori, JCAP **1808**, no. 08, 047 (2018), [arXiv:1807.06335 [hep-th]].
- [20] P. Jirouek and A. Vikman, JCAP **1904**, 004 (2019), [arXiv:1811.09547 [gr-qc]].
- [21] M. A. Gorji, S. Mukohyama and H. Firouzjahi, JCAP **1905**, no. 05, 019 (2019), [arXiv:1903.04845 [gr-qc]].
- [22] A. H. Chamseddine, V. Mukhanov and A. Vikman, JCAP **1406**, 017 (2014), [arXiv:1403.3961 [astro-ph.CO]].
- [23] L. Mirzaghali and A. Vikman, JCAP **1506**, 028 (2015), [arXiv:1412.7136 [gr-qc]].
- [24] S. Ramazanov, F. Arroja, M. Celoria, S. Matarrese and L. Pilo, JHEP **1606**, 020 (2016), [arXiv:1601.05405 [hep-th]].
- [25] A. Ijjas, J. Ripley and P. J. Steinhardt, Phys. Lett. B **760**, 132 (2016), [arXiv:1604.08586 [gr-qc]].
- [26] H. Firouzjahi, M. A. Gorji and S. A. Hosseini Mansoori, JCAP **1707**, 031 (2017), [arXiv:1703.02923 [hep-th]].
- [27] S. Hirano, S. Nishi and T. Kobayashi, JCAP **1707**, no. 07, 009 (2017), [arXiv:1704.06031 [gr-qc]].
- [28] Y. Zheng, L. Shen, Y. Mou and M. Li, JCAP **1708**, no. 08, 040 (2017), [arXiv:1704.06834 [gr-qc]].
- [29] M. A. Gorji, S. A. Hosseini Mansoori and H. Firouzjahi, JCAP **1801**, no. 01, 020 (2018), [arXiv:1709.09988 [astro-ph.CO]].
- [30] D. Langlois, M. Mancarella, K. Noui and F. Vernizzi, JCAP **1902**, 036 (2019) doi:10.1088/1475-7516/2019/02/036 [arXiv:1802.03394 [gr-qc]].
- [31] A. Ganz, N. Bartolo and S. Matarrese, arXiv:1907.10301 [gr-qc].
- [32] R. Myrzakulov, L. Sebastiani, S. Vagnozzi and S. Zerbini, Class. Quant. Grav. **33**, no. 12, 125005 (2016), [arXiv:1510.02284 [gr-qc]].
- [33] V. K. Oikonomou, Int. J. Mod. Phys. D **25**, no. 07, 1650078 (2016), [arXiv:1605.00583 [gr-qc]].
- [34] C. Y. Chen, M. Bouhmadi-Lpez and P. Chen, Eur. Phys. J. C **78**, no. 1, 59 (2018), [arXiv:1710.10638 [gr-qc]].

- [35] X. z. Li, X. h. Zhai and P. Li, arXiv:1807.08270 [gr-qc].
- [36] G. G. L. Nashed, W. El Hanafy and K. Bamba, JCAP **1901**, no. 01, 058 (2019), [arXiv:1809.02289 [gr-qc]].
- [37] A. Sheykhi and S. Grunau, arXiv:1911.13072 [gr-qc].
- [38] K. Izumi and S. Mukohyama, Phys. Rev. D **81**, 044008 (2010) doi:10.1103/PhysRevD.81.044008 [arXiv:0911.1814 [hep-th]].
- [39] D. Blas, O. Pujolas and S. Sibiryakov, JHEP **0910**, 029 (2009) doi:10.1088/1126-6708/2009/10/029 [arXiv:0906.3046 [hep-th]].
- [40] E. Barausse, T. Jacobson and T. P. Sotiriou, Phys. Rev. D **83**, 124043 (2011) doi:10.1103/PhysRevD.83.124043 [arXiv:1104.2889 [gr-qc]].